β-Hairpin Folding by a Model Amyloid Peptide in Solution and at an Interface

Volker Knecht*

Max Planck Institute of Colloids and Interfaces, Science Park Golm, 14424 Potsdam, Germany

Received: March 27, 2008

The development of specific agents against amyloidoses requires an understanding of the conformational distribution of fibrillogenic peptides at a microscopic level. Here, I present molecular dynamics simulations of the model amyloid peptide LSFD with sequence LSFDNSGAITIG-NH_2 in explicit water and at a water/vapor interface for a total time scale of $\sim$1.8 μs. An extended structure was used as initial peptide configuration. At $\sim$290 K, solvated LSFD was kinetically trapped in diverse misfolded β-sheet/coil conformations. At 350 K, in contrast, the same type II′ β-hairpin in equilibrium with less ordered but also U-shaped conformations was observed for the core residues DNSGAITI in solution and at the interface in multiple independent simulations. The most stable structural unit of the β-hairpin was the two residue turn (GA). The core residues exhibited a well-defined folded state in which the β-hairpin was stabilized by a hydrogen bond between the side chain of Asn-385 and the main chain carbonyl group of Gly-387. My results suggest that β-sheet conformations indicated from previous Fourier-transform infrared spectroscopy measurements immediately after preparation of the peptide solution may not arise from protofilaments as speculated by others but are a property of LSFD monomers. In addition, combined with previous results from X-ray scattering, my findings suggest that interfacial aggregation of LSFD implies a transition from U-shaped to extended peptide conformations. This work including the first simulations of reversible β-hairpin folding at an interface is an essential step toward a microscopic understanding of interfacial peptide folding and self-assembly. Knowledge of the main conformation of the peptide core may facilitate the design of possible inhibitors of LSFD aggregation as a test ground for future computational therapeutic strategies against amyloid diseases.

Introduction

Amyloidoses such as Alzheimer's are associated with the conversion of globular proteins from a soluble and functional form into a β-rich structure[1] that often tends to precipitate in the form of fibrils.[2] The surface and membrane activity of amyloid species and the observation that hydrophobic surfaces can induce β-sheet formation suggest that cell membrane surfaces could serve as a point for oligomerization and fibril nucleation.[3–5] The toxicity of amyloid species is attributed to their fibrillar or oligomeric but not to monomeric forms.[6] A possible therapeutic strategy against amyloid diseases could thus be the use of agents which prevent aggregation of amyloid species.[7] To minimize side effects, such agents must be effective at low concentrations and thus bind to amyloid species via specific interactions. For the design of such compounds, detailed knowledge of the structure of the respective fibrillogenic species is essential.

Experimentally, it is extremely difficult to study fibrillogenic species in atomic detail just because of their tendency to aggregate.[8] Instead, theoretical methods, specifically, molecular dynamics (MD) simulation techniques must be employed to computationally model the process by which these species sample conformational space. MD simulations which are based on iteratively solving Newton's equations of motion to propagate the system in time and semiempirical force fields to describe interatomic interactions[9] can provide highly detailed information on the properties of fibrillogenic peptides in solution. Existing MD simulations have suggested that fibrillogenic peptides primarily form coil or β-sheet conformations in the monomeric state.[10–20] In some of the studies, the peptides were described using simplified models, and/or the solvent was modeled implicitly.[18,21,22] While such models can extend the time and length scales of the simulations for a given computational cost, they can provide at best only a qualitative picture of the underlying process. To obtain a detailed quantitative understanding of the conformational distribution of fibrillogenic peptides, the use of a full atomistic description of the peptide and its solvent environment is required. The computational expense of full atomistic calculations, though, implied that many previous studies were biased from the initial configuration[12,23–25] or that the (un)folding events observed in the simulations were irreversible such that neither the relative populations of alternative conformational states nor even a main conformation could be assessed.[10,13,15,17,19,20] Thus, specific techniques must be used to facilitate sampling of conformational space and currently only relatively short peptides can be studied in a reliable manner.[14,16] Such studies can give insights into the universal, nonsequence dependent behavior of amyloid peptides[5] and pave the way for reliable simulations of larger peptides with direct medical relevance that, because of ongoing advances in both hard- and software, are expected to be possible in the near future.

I have chosen an amidated 12-amino acid peptide denoted as LSFD[5] as a model system. Its sequence corresponding to residues 381−392 of the cell attachment fiber protein of human adenovirus Ad2[26] shown in Figure 1 (top) comprises both hydrophilic and hydrophobic residues. An atomic detailed structural model based on X-ray data for the LSFD sequence in the parent protein is depicted in Figure 1 (bottom). Here, three-residue β-strands are formed by residues 382−384 (SFD) and 388−390 (AIT), connected by a loop formed by residues 385−387 (NSG). LSFD forms amyloid-like fibrils in aqueous solution (pH 7) as evident from electron microscopy, Congo

* Corresponding author. E-mail: vknecht@mpikg.mpg.de.

10.1021/jp8026513 CCC: $40.75
Published on Web 07/02/2008

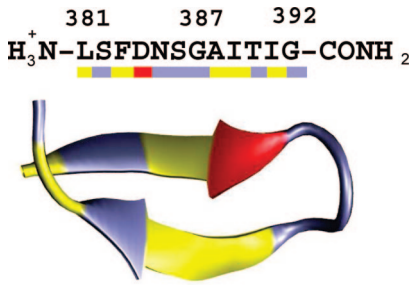

Figure 1. LSFD, a fibrillogenic peptide corresponding to residues 381−392 of the cell attachment protein of human adenovirus Ad2. Top: amino acid sequence. Bottom: structural model for the protein-embedded sequence based on X-ray data. The color code distinguishes between hydrophobic (yellow), hydrophilic (blue), and acidic residues (red).

red binding, infrared spectroscopy, and X-ray fiber diffraction.[26] Remarkably, the tendency of LSFD to form amyloid fibrils is significantly higher than that of the amyloid beta (A β; 1−40) peptide related to Alzheimer's disease.[5] Spread at a water−air interface, LSFD forms β-rich monolayer films with crystalline order that are stable upon transfer to a quartz substrate. Due to their high order, LSFD monolayers on quartz have been proposed as a possible means to produce nanometer surface patterns and nucleation sites that could be used to induce technologically relevant crystalline nanostructures.[5,28] Fourier-transform infrared (FTIR) spectra of LSFD in (deuterated) water indicate significant β-sheet together with turn and random coil content immediately after preparation of the solution. However, it is not clear to which extend this secondary structure corresponds to mono- or oligomers.[26] No data are available for the structure of LSFD at a water/air interface at low surface densities.

Here, I present MD simulations of LSFD in explicit water and at a water/vapor interface (vapor modeling air) revealing the conformational distribution of the peptide at a microscopic level. The water/vapor interface can be viewed as a simple model for a water/membrane interface. The absence of zwitterionic headgroups normally lining a water/membrane interface facilitated efficient sampling of conformational space. Starting from an extended peptide configuration, the solvated peptide sampled diverse apparently misfolded β-sheet/coil conformations at room temperature ($\sim$ 290 K). At 350 K, in contrast, the same type II′ β-hairpin in equilibrium with less ordered but also U-shaped conformations was observed for the core residues DNSGAITI in solution and at the interface in multiple independent simulations. In particular, this work includes the first simulations of reversible β-hairpin folding at an interface. Detailed knowledge of the structure and dynamics of LSFD monomers is a necessary step to understand the nucleation of the bidimensional crystals formed by this peptide relevant for possible nanotechnological applications. In addition, knowledge of the predominant conformation of LSFD could facilitate the design of compounds with complementary surface and, thus, high binding affinity to the peptide, thereby inhibiting aggregation efficiently. A successful test of this approach for the model peptide chosen here might open the perspective to a therapeutic strategy against amyloid diseases based on molecular dynamics and rational drug design.

Methods

Simulation Setups. The LSFD peptide was simulated in bulk water and at a water/vapor interface under periodic boundary

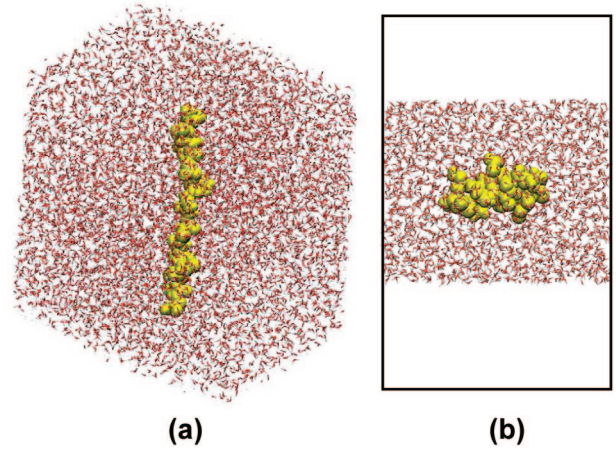

Figure 2. Initial configurations of systems simulated. (a) LSFD in water. Here, an extended structure was used as initial peptide configuration. (b) LSFD at water/vapor interface. Here, a compact structure (β-hairpin) was used as initial peptide configuration, and the peptide was placed in the center of the water slab. The peptide is shown as yellow spheres; water is shown as sticks indicating oxygen (red) and hydrogen atoms (white). In (b), the simulation box is indicated by a black frame.

conditions using molecular dynamics simulations. The initial configurations of the systems simulated are shown in Figure 2. The peptide modeled amidated and in an extended initial configuration was placed in an octahedral box of edge length 6.6 nm such that the distance between the peptide and the boundary of the box was at least 1.2 nm. The remaining space was filled with 7066 water molecules to model the peptide in solution (Figure 2a). The system was energy minimized using steepest descent to remove possible overlap of atoms. The solvent was equilibrated in a subsequent simulation of 1 ns, keeping the atoms of the peptide close to their initial positions using a harmonic potential. To model the peptide at a water/vapor interface, the peptide in a compact (β-hairpin) conformation was placed in a rectangular box of size 4.5 × 4.5 × 3.6 nm^3, and the remaining space was filled with 2331 water molecules. After energy minimization and solvent equilibration as described above, the box was extended to a length of 9 nm in z direction to create a vapor phase (Figure 2b). LSFD in bulk water was simulated 3 times for 50 ns at 293 K and was simulated 3 times for at least 200 ns at 350 K using different sets of initial velocities. One of the simulations at 350 K was extended to 300 ns. For LSFD at the interface, three 300 ns simulations at 350 K using different velocity distributions were performed. The motivation for choosing the given temperatures was to mimic experimental conditions (293 K) or to enhance sampling (350 K), respectively.

The peptide was described using the GROMOS96−43a1 force field[29] in which CH_i groups (i = 1, 2, 3) are described using united atoms. Water molecules were represented by the three-site simple point charge (SPC) model.[30] All simulations were performed using the GROMACS[31] simulation code. The covalent bond lengths were constrained using the LINCS[32] (peptide) or SETTLE[32] method (water molecules), respectively. In addition, the masses of atoms attached to hydrogens were redistributed so as to increase the mass of the hydrogen atoms simulated explicitly. This eliminates high frequency motions of the hydrogens which allows the use of a time step of 4 fs.[33] Even though this slightly alters the kinetic properties of the system, it does not affect its structural properties. It has been found that even 5 fs time steps did not affect the populations

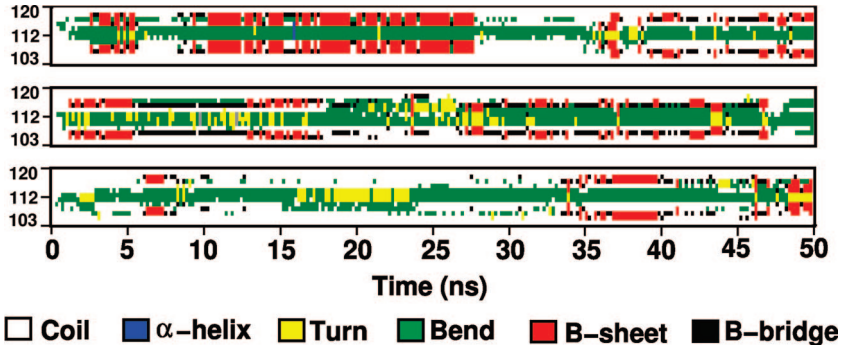

Figure 3. Formation of β-sheets for LSFD peptide in water at 293 K. Three 50 ns simulations were performed starting from the same extended configuration but for different initial velocity distributions. The time evolution of the secondary structure of the peptide during the three simulations based on an analysis of hydrogen bonds in the peptide main chain using the program DSSP[38] is shown. Here, the vertical coordinate represents the residue number which is plotted against time, and the secondary structure is color-coded.

of alternative conformational states of peptides significantly.[34] The temperature was controlled by separately coupling the peptide and the solvent to an external heat bath using a Berendsen thermostat[35] with a coupling constant of 0.1 ps. For the solvated peptide, an average pressure of 1 bar was maintained by scaling the box size isotropically using a Berendsen barostat[35] with a coupling constant of 1 ps. A fixed box size was used for the water/vapor interface. Full electrostatic interactions were computed using the particle mesh Ewald technique[36] with tinfoil boundary conditions.[37] Snapshots were saved every 20 ps for further analysis.

Analysis. The secondary structure of the peptide was determined on the basis of an analysis of hydrogen bonds within the main chain of the peptide according to the following definitions.[38] An n-turn is characterized by a hydrogen bond between residues i and $i + n$. Two or more consecutive n-turns form an n-helix. The case $n = 4$ indicates an α-helix; $n = 3$ indicates a 3_{10}-helix, and $n = 5$ indicates a π-helix. Two strands joined by hydrogen bonds involving alternating residues on each participating strand indicate a β-sheet, if each strand contains two or more residues, or indicate a β-bridge, if each strand contains only a single residue. A strongly curved region in the peptide backbone is called a bend. Regions showing neither of these secondary structure motifs are denoted as coil. The content of selected secondary structure motifs of the individual residues of the peptide was determined by averaging over the 3 trajectories at 350 K. Here, the initial 5 or 10 ns of the trajectories of the solvated or interfacially adsorbed peptide, respectively, were omitted for equilibration. For the peptide at the interface, in addition, periods during which the peptide transiently left the interface (which happened 4 times within the 900 ns simulated) were omitted from analysis as well. In these analyses, the coil, β-sheet, turn, and bend content were considered.

The Daura cluster analysis method[39] was used to cluster the configurations sampled in the trajectories at 350 K. Here, the trajectories of the solvated and the interfacially adsorbed peptide were analyzed separately. First, I calculated the root-mean-square deviation (rmsd) of either all atoms or only main chain atoms of residues 384−391 between all pairs of configurations (residues 381−383 and 392 exhibiting more than 60% coil conformation were excluded from analysis). Pairs of configurations with an rmsd of less than 0.14 nm were considered to be neighbors. The configuration with the largest number of neighbors, together with the neighbors, was taken to form the first cluster and eliminated from the pool of structures. This process was repeated until no configurations remained in the pool. The rmsd cutoff of ≤0.14 nm was chosen on the basis of the overall rmsd distribution showing bimodal behavior and taken equal to the location of the respective local minimum of the distribution. For the central configuration of the most populated cluster, hydrogen bonds were identified on the basis of a geometric criterion. A hydrogen bond was considered to be formed if the distance between hydrogen and acceptor was less than 0.24 nm and the angle formed by donor, hydrogen, and acceptor was less than 35°.

For each solvated and interfacially adsorbed peptide at 350 K, the average surface area of the peptide was analyzed. Here, the total "solvent accessible" surface area (SASA) of a given peptide configuration, defined as the area traced out by the center of a probe sphere representing a water molecule as it is rolled over respective groups of the solute, was calculated on the basis of an algorithm by Connolly[40] using the program g_sas from the GROMACS package.[31] The number of contacts between water oxygen and peptide heavy atoms for the individual residues and averaged over the residues was determined by averaging over the respective trajectories. Two atoms were considered to be in contact if their distance was below 0.43 nm. Error intervals were obtained by calculating the standard error of the estimates from three independent simulations using different initial velocity distributions. For LSFD at the interface, the density of water and selected peptide groups as a function of the distance normal to the interface, normalized to one, were determined using a 0.01 nm bin width. The profiles were smoothed using a Gaussian filter of 0.03 nm bin width. Here, the origin of the distance scale was set to the point at which the water density equaled half the bulk density. All simulations were performed on AMD Opteron 2.0 GHz dual processor/dual core nodes. The VMD[41] and MOLMOL[42] programs were used for trajectory visualization and graphical structure analysis.

Results

Reversible Folding at Elevated Temperature. As shown in Figure 2a, simulations were started from an extended configuration of LSFD placed in explicit water. Simulations at 293 K to mimic experimental conditions and at 350 K to enhance the sampling were performed. Figure 3 shows the evolution of secondary structure for the peptide at 293 K. In the initial phase of the simulations, bends (green) and, to a lesser degree, turns (yellow) were formed in the center of the peptide. Subsequently, β-sheets (red) formed, resulting in strand-loop-strand or β-hairpin conformations, most of which dissolved again during the simulations. The presence of turns and β-sheets is in agreement FTIR spectra immediately recorded after preparation of the LSFD peptide solution,[26] suggesting that these spectra

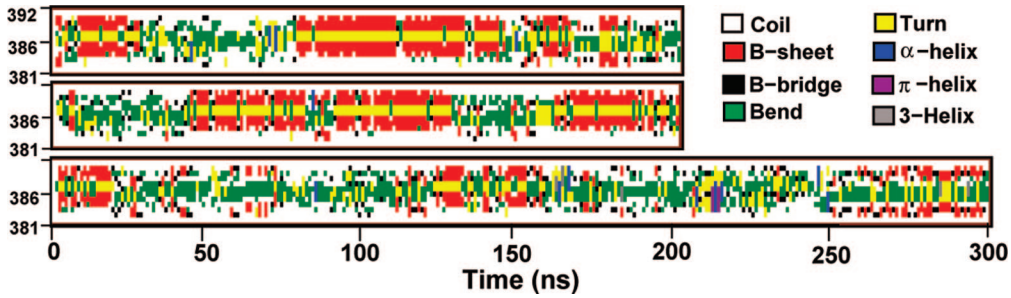

Figure 4. Reversible β-hairpin folding for LSFD peptide in water at 350 K. Three independent simulations were started from the same extended configuration but from different initial velocity distributions. The representation is similar to that chosen in Figure 3.

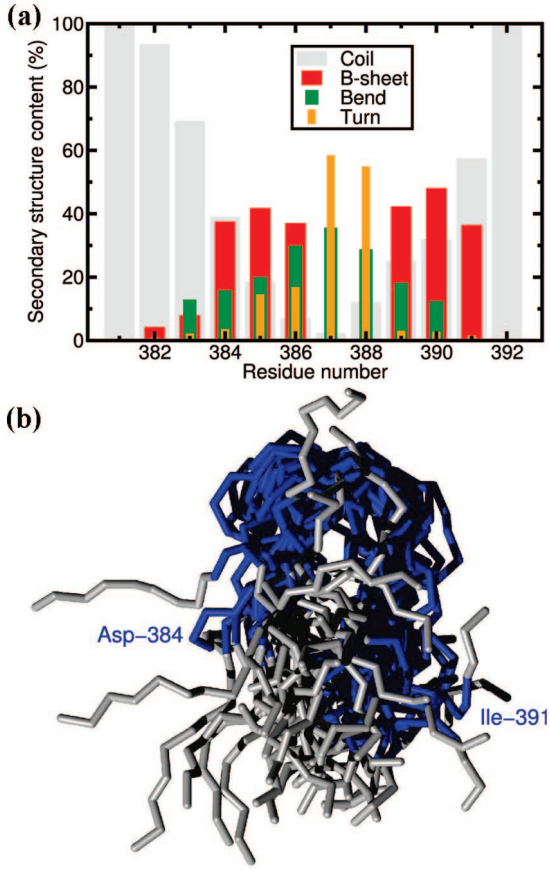

Figure 5. Structure versus conformational flexibility for LSFD in water at 350 K. (a) Secondary structure content per residue. (b) Conformational flexibility. The central backbone configurations of the 32 largest clusters consisting of 75% of the configurations are shown in stick representation. Residues 384−391 are shown in blue; residues 381−383 and 392 are depicted in gray.

may arise from monomers. Various β-sheets containing different residues were observed, and a predominant conformation was not obvious from the trajectories. This was different at 350 K, as shown in Figure 4. Here, an increased amount of β-sheet and turn conformations was detected, and the same β-hairpin consisting of residues 384−391 was formed reversibly in 3 independent simulations. This suggests that the peptide was in an equilibrium between β-hairpin and disordered conformations.

Structure versus Flexibility. Figure 5a shows the average coil, β-sheet, bend, and turn content per residue for LSFD at 350 K. A high turn and bend content was observed for Gly-387 and Ala-388 (the sum of the turn and bend content being 94% for Gly-387 and 84% for Ala-388, respectively). Lower but appreciable turn and bend content was observed for residues 384−386. Significant β-sheet content (∼40%) was observed for residues 384−386 and 389−391. Low β-sheet content (∼5%) was detected for residues 382 and 383. Residues 381−383 and 392 adopted mainly coil conformations (>60%).

To discretize the conformational space of the peptide, the peptide configurations of the trajectories at 350 K were subjected to a cluster analysis based on the main chain backbone configurations of residues with less than 60% coil content (residues 384−391, denoted henceforth as core) as described in the methods section. The 34 252 configurations considered formed 766 clusters. The central configurations of the 32 largest clusters containing 75% of the configurations are shown in Figure 5b. Whereas the terminal residues 381−383 and 392 (gray) were highly flexible, the core formed U-shaped conformations with low structural variability. The highly bent region contained Gly-387 and Ala-388 and, with lower probability, residues 384−386. These observations are consistent with the secondary structure profiles along the peptide sequence described above. Despite the defined overall topology of the core, typically local rearrangements resulted in different coil or β-bridge structures, β-sheets that consisted of different sets of residues, and even 1.2% α-helical conformations (residues 385−390).

***β*-Hairpin.** The largest configurational cluster included 34%, while the second largest cluster comprised only 7% of the configurations, indicating a well-defined predominant main chain conformation of the core (also suggested from the time evolution of the secondary structure of the trajectories shown above). The central configuration of the largest cluster, a β-hairpin, is shown in Figure 6 (top) in two different representations. As evident from Figure 6a, three-residue β-strands are formed by residues 384−386 (DNS) and residues 389−391 (ITI), while the turn is formed by residues 387 and 388 (GA). The backbone torsion angles of the turn were $\phi = 80°$ and $\psi = -89°$ for Gly-387 and $\phi = -114°$ and $\psi = -28°$ for Ala-388. The turn was thus of type II′. Note that the conformation of the backbone of residue 387 is possible for glycine having no side chain, while forbidden for all other amino acids due to steric side chain interactions. Figure 6b shows that hydrogen bonds are formed between the backbone NH and C═O groups of Asp-384 and Ile-391, Ser-386 and Ile-389, and Ile-389 and Ser-386, as well as Ile-391 and Asp-384. Note that the main conformation shown in Figure 6 is different from the structural model for the protein-embedded fragment (Figure 1 bottom). This suggests that tertiary contacts of the fragment with the rest of the protein codetermine the conformation of the protein-embedded fragment.

To determine the essential side chain conformers for the type II′ β-hairpin, the 11 601 configurations of the β-hairpin ensemble were subjected to a further cluster analysis in which (besides the main chain) also the side chains of residues 384−391 were included. From the 116 clusters formed, the largest cluster included 77%, while the second largest cluster comprised 5% only. The side chains were thus significantly more flexible than

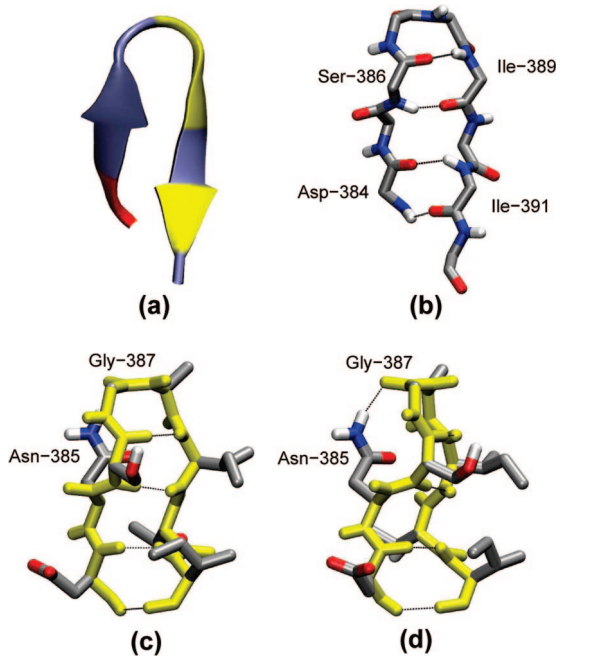

Figure 6. Type II′ β-hairpin, main conformation for residues 384−391 of LSFD in water at 350 K as suggested from a cluster analysis. The same configuration is depicted in ribbon (a) or stick representation of the backbone (b) or backbone plus side chains from different perspectives (c,d). In (a), the same color code as in Figure 1 is used. In (b−d), colors indicate carbon (gray), nitrogen (blue), oxygen (red), and hydrogen atoms (white), and hydrogen bonds are depicted as dotted lines. In (c,d), the backbone is shown in yellow.

the main chain but exhibited a well-defined predominant conformation as well, defining a folded state for the core of the isolated LSFD peptide shown in Figure 6c,d. Here, a hydrogen bond is formed between the side chain of Asn-385 and the carbonyl group of Gly-387 that may stabilize the β-hairpin conformation. The respective coordinates of the peptide core are provided as Supporting Information.

LSFD at Water/Vapor Interface. To investigate effects of the environment on the structure and dynamics of LSFD, the folding of LSFD at a water/vapor interface was studied. As shown in Figure 2b, LSFD modeled in a compact conformation (β-hairpin conformation shown in Figure 6a) placed in a water slab in contact with vapor was used as the initial configuration. Three independent simulations at 350 K using the same initial configurations but different sets of initial velocities were performed. Within the initial 10 ns of each of the trajectories, the peptide was adsorbed at one of the interfaces. However, the peptide transiently left the interface for a few nanoseconds once or twice in each of the simulations. These parts of the trajectory, together with an initial 10 ns equilibration period, were omitted whenever ensemble averages were determined. Figure 7 shows the time evolution of the rmsd of the main chain configuration of the core (residues 384−391) from the β-hairpin configuration shown in Figure 6a, revealing that multiple un- and refolding events were observed for each trajectory. This observation suggested that the predominant main chain conformation of the peptide at the interface was similar to that in bulk water and in equilibrium with unfolded conformations. Likewise, the secondary structure content of the individual residues was similar to that in bulk water (data not shown). Again, the core formed U-shaped conformations with low structural variability, whereas the terminal residues 381−383 and 392 were highly flexible. A cluster analysis of the 42 152 configurations considered based on the rmsd of the main chain atoms of residues

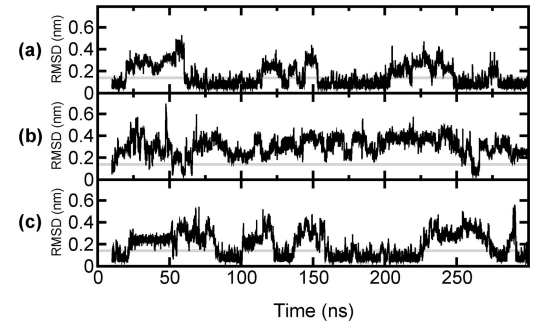

Figure 7. Reversible folding of LSFD at a water/vapor interface at 350 K. The root-mean-square deviation of the main chain atoms of residues 384−391 from the β-hairpin configuration shown in Figure 6a as a function of time in three independent simulations is depicted. The gray line indicates the rmsd cutoff used to estimate the population of the β-hairpin conformation.

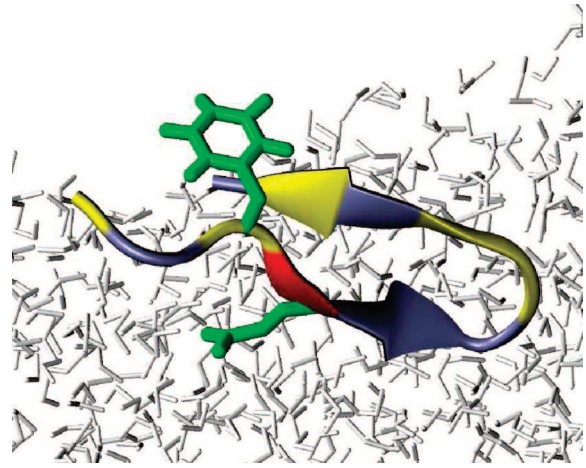

Figure 8. LSFD at a water/vapor interface at 350 K. The representation is similar to that chosen in Figure 1 (bottom) and Figure 6a. The side chains of Phe-383 and Asp-384 are shown as green sticks. Water molecules are depicted as white sticks.

384−391 yielded 482 clusters where the largest cluster consisted of 36% and the second largest cluster comprised only 8% of the configurations. The predominant backbone conformation of the core was a β-hairpin similar to that in water. Figure 8 shows a configuration of LSFD at a water/vapor interface, the peptide core adopting its main (β-hairpin) conformation. The peptide long axis is parallel to the interface. Hydrophobic residues (yellow) point toward the vapor phase. The phenylalanine side chain (green aromatic ring) is in immediate contact with vapor. Hydrophilic residues (blue and red), in particular, the aspartate side chain (green branched chain), point toward the water phase.

Several aspects suggested from this configuration were analyzed quantitatively by averaging over the three trajectories as indicated in the methods: (i) the peptide orientation, (ii) the distribution of various groups normal to the interface, and (iii) the number of interatomic contacts between the individual residues and the water. To analyze the peptide orientation, the peptide axis was defined as follows. In consideration that the peptide core consisting of residues 384−391 adopted U-shaped conformations, the peptide axis was defined as the vector connecting the center of mass of residues 384 and 391 (tips of the U-shape) with that of residues 387 and 388 (turn/bend region). The angle between this axis and the interface normal was on average 88° with a standard deviation of 24°. Thus, the peptide was on average parallel to the interface.

Figure 9a shows the distribution of water, (polar) backbone atoms, polar side chains, and nonpolar side chains (plus C_α

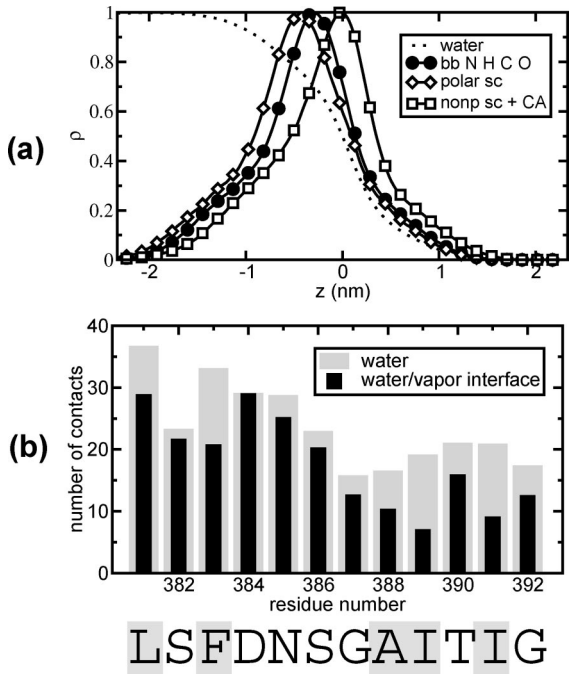

Figure 9. Peptide location and peptide−water contacts at a water/vapor interface. (a) Density distribution of water (dotted line) and peptide (solid lines) normal to water/vapor interface. For the peptide, amide group (filled circles), backbone C_α atoms plus nonpolar side chains (filled circles), and nonpolar side chains (squares) are distinguished. (b) Number of interatomic contacts between the peptide and the water (heavy atoms) per residue for LSFD at a water/vapor interface (black) and in bulk water (gray). The amino acid sequence is given with hydrophobic residues indicated in gray.

atoms) normal to the interface. The water density (dotted line) shows a smooth transition from bulk to vapor with a width of ~2 nm. The peptide backbone (filled circles) is located at the water side of this transition region. The full width at half-maximum of this distribution of ~1 nm reflects the alignment of the peptide with the interfacial plane. Relative to the distribution of backbone atoms, the distributions of polar (diamonds) and nonpolar side chains (squares) are shifted toward the water or vapor phase, respectively, the shift being more pronounced for the nonpolar side chains. This indicates that polar and nonpolar side chains on average pointed toward the water and the vapor phase, respectively.

The number of interatomic contacts between peptide and water were 216 ± 1 at the interface compared with 288 ± 1 in solution, although the average surface areas of the peptide in the two environments were similar (11.62 ± 0.08 nm^2). This indicates that parts of the peptide were in immediate contact with the vapor phase (as also suggested from Figure 8). Figure 9b shows the number of interatomic contacts between the water and the individual residues of the peptide in solution and at the interface. Except for Asp-384 for which no difference between the two environments was detected, an overall decrease in the number of contacts was observed. The decrease correlated with the hydrophobicity of the residue and was most pronounced for Phe-383, Ile-389, and Ile-391. These observations are consistent with the view that the stabilization of the peptide at the interface arises from the hydrophobic effect.

To recall, the predominant main chain conformation was a type II′ β-hairpin similar to that found in water as suggested from a cluster analysis based on the main chain configurations of residues 384−391. The largest cluster from this analysis was subjected to a second cluster analysis based on the configurations

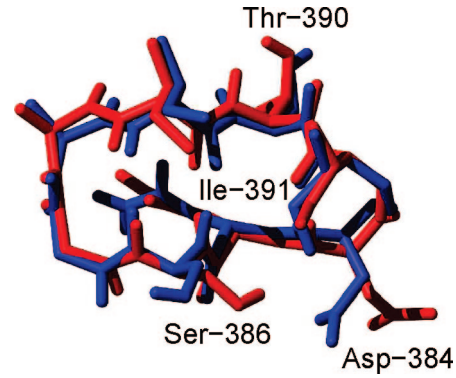

Figure 10. Comparison of the predominant conformations of residues 384−391 in water (blue) and at a water/vapor interface (red) in stick representation.

of the main and side chains of the core residues. The 15 140 configurations considered formed 152 clusters. The largest and second largest cluster consisted of 63 and 7% of the configurations, respectively. Again, the side chains were thus significantly more flexible than the main chain but exhibited a well-defined predominant conformation as well, representing a folded state for the core of the isolated LSFD peptide. Figure 10 compares the main conformation of the core residues at the interface (red) and that in solution (blue). Remarkably, the conformations are very similar and differ only in the side chain rotamers of Asp-384, Ser-386, Thr-390, and Ile-391.

Discussion

LSFD in Water. At both temperatures (293 and 350 K), monomeric LSFD in water was found to sample β-hairpin or strand-loop-strand as well as disordered conformations. At room temperature (293 K), various β-sheets that contained different residues where observed. At the elevated temperature (350 K), in contrast, the same type I′ β-hairpin conformation was formed by residues 384−391 denoted as peptide core (turn at residues Gly-387 and Ala-388) in three independent simulations. The difference in the conformational distributions between the two temperatures most likely arised from a difference in sampling efficiency. Whereas the simulations at room temperature (293 K) suffered from kinetic trapping of misfolded structures, reversible folding on the simulation timescales was possible at the elevated temperature. In a previous simulation study, the free energy landscape of another β-hairpin forming peptide was found to be rugged at room temperature while smooth and funnel-like at about 360 K.[43] Heating is not expected to change the structure but only the population of the main conformation of a peptide. This may be illustrated at the fibrillogenic A β (25−35) fragment of the amyloid β peptide associated with Alzheimer's disease.[44,45] Similar to LSFD at elevated temperature, A β (25−35) forms disordered and two specific β-hairpin conformations when solvated in water as suggested from simulations.[16] As indicated from the β-sheet or turn content along the amino acid sequence at different temperatures, increasing the temperature from 300 to 350 K did not change the secondary structure pattern but only led to a decrease in the population of the β-hairpin conformations by a factor of ~0.7. Likewise, the conformational distribution of LSFD at room temperature is expected to be similar to that at 350 K, and the main difference relevant here is expected to be a stronger population of the β-hairpin conformation. In conclusion, I expect the type II′ β-hairpin conformation of residues 384−391 shown in Figure 6 to be the main conformation not only at 350 K but

also at 293 K. A lower bound for the population of the β-hairpin conformation suggested from my simulation results is ~40%. As temperatures around 293 K correspond to conditions of experiments on LSFD reported previously,[5,26,46] my results might be related to available experimental data, as done in the following.

Significant β-hairpin conformations for LSFD in water are consistent with β-sheet and turn structure indicated from FTIR measurements on LSFD dissolved in (deuterated) water recorded immediately after preparation of the solution.[26] It was speculated originally that the β-sheet structures detected in these experiments could arise from intermolecular hydrogen bonding and indicate the presence of protofilaments. My simulations, in contrast, suggest that the presence of oligomeric species is not required for β-sheet structure which could arise from intramolecular hydrogen bonding instead. The latter may be formed quickly, while formation of protofilaments is expected to involve a significant lag phase. It is therefore likely that β-sheet content detected immediately after solvating the peptides may mainly arise from monomers. This hypothesis might be tested experimentally by recording respective FTIR or circular dichroism (CD) spectra at various peptide concentrations.

Remarkably, the main conformation of LSFD in water revealed from my simulations is different from the conformation of the protein-embedded sequence suggested from X-ray data.[27] Though β-hairpins with three-residue β-strands are formed in both cases, the conformations differ in (i) the residues forming the β-strands and (ii) the number of residues in the β-hairpin loop (three for the protein-embedded and two for the isolated sequence). This difference in conformation suggests that the conformation of the protein-embedded sequence is influenced by tertiary contacts with the rest of the protein and thus is not an independent folding unit. The most stable structural unit of the β-hairpin formed by LSFD is the two-residue turn with 58 or 55% turn and 94 or 84% turn and bend content for Gly-387 and Ala-388, respectively. This suggests that the propensity of a Gly-Ala sequence to form turns or bends, in particular, the high flexibility of the glycine residue, leads to an overall U-shaped topology of the peptide backbone and facilitates the formation of an intramolecular β-sheet. Mutating the glycine into alanine is thus expected to decrease the average β-sheet content, whereas alanine substitutions at other sites are not expected to have a strong impact on the secondary structure of LSFD. Likewise, the type II′ turn in the predominant β-hairpin conformations of A β (25−35) consists of a glycine and an alanine residue (Gly-29 and Ala-30) and provides the most stable structural unit of these β-hairpin conformations as suggested from previous simulations.[16] The effect of alanine substitutions of the glycine or other residues is expected to be similar to that indicated for LSFD above. These predictions could be verified experimentally using FTIR or CD spectroscopy—assuming that the conformation of LSFD in fibrils adopts the same conformation as that of the protein-embedded sequence, various structural models for LSFD fibrils were proposed previously.[26] My results revealing monomeric LSFD to exhibit considerable conformational plasticity and a main conformation different from the protein-embedded sequence suggest such models to be overly simplistic and possibly misleading.

A folded state of the peptide core in which the β-hairpin conformation of the main chain is stabilized by a hydrogen bond between the side chain of Asn-385 and the carbonyl group of Gly-387 is suggested. Knowledge of the folded state might facilitate the design of a compound with complementary surface and high binding affinity to the peptide as a possible inhibitor of peptide aggregation. In the unfolded state, intramolecular hydrogen bonds are typically dissolved, but an overall U-shaped conformation of the main chain is retained and only local rearrangements are required to restore the folded state. Thus, at any encounter between the peptide and an agent targeting the folded state of the core, binding might be probable and occur either by a key-lock or by an induced fit mechanism[47] depending on the current peptide conformation. The predominance of U-shaped conformations in the unfolded state supports the conclusion from previous studies of non-natural peptides that the denatured state of peptides consists of far less conformations than could be expected from the number of conformational degrees of freedom involved.[48]

LSFD at Water/Vapor Interface. After previous simulations of reversible β-hairpin folding in explicit solvent including studies of amyloid peptides by Daidone et al.,[14] I present the first simulations of reversible β-hairpin folding at an interface. Hence, this study is an essential step toward a microscopic understanding of interfacial peptide folding and self-assembly. My results suggest that LSFD monomers at a water/vapor interface exhibit a conformational distribution similar to that in solution. In particular, the core residues mainly form U-shaped conformations and their predominant conformation is a β-hairpin similar to that in bulk water differing in a few side chain rotamers only. LSFD monomers are oriented parallel to the interface with hydrophilic or hydrophobic side chains pointing to the water or vapor phase, respectively. Although the surface area of the peptide is similar to that in bulk water, the number of intermolecular contacts between peptide and water is reduced significantly, especially for hydrophobic side chains. This indicates that LSFD is in immediate contact with the vapor phase and that the interfacial position of LSFD is stabilized by hydrophobic effects. The conformational behavior of LSFD contrasts with the conformational polymorphism of the model amyloid peptide B18 in monomeric form that exhibits β-sheet, turn, and coil conformations in water but exhibits partially α-helical conformations at a water/vapor interface as observed in previous MD simulations.[19] This gives an example for a sequence-dependent property of amyloid peptides.

Simulation results on peptide monomers at a water/vapor interface corresponding to a monolayer in the gas phase are particularly valuable; to study peptides at low surface densities experimentally is difficult. Experimental data, though, are available for condensed LSFD monolayers at a water/air interface showing that peptides are extended and form antiparallel intermolecular β-sheets oriented parallel to the interface and forming crystalline domains.[5] The preformed β-strand conformations, in-plane alignment, and preferential partitioning of hydrophilic and hydrophobic side chains between the two phases implies some preorganization of monomers that might facilitate their assembly to the bidimensional crystalline domains observed in experiment. Aggregation, though, appears to involve a transition from intra- to intermolecular hydrogen bonding, together with a change from U-shaped to extended and from β-sheet/coil to pure β-sheet conformations.

Conclusion

My MD simulations in conjunction with elevated temperatures to facilitate sampling reveal an equilibrium between type II′ β-hairpin and U-shaped coil conformations for the model amyloid peptide LSFD in water or at a water/vapor interface. My results suggest that LSFD at the interface is aligned with the interfacial plane and that its hydrophobic side chains point toward the vapor phase, thus being partially desolvated. This

work includes the first all-atom simulations of reversible β-hairpin folding at an interface. It is thus an essential step toward a microscopic understanding of interfacial peptide folding and self-assembly which is of high nanotechnological, biological, and medical relevance. Knowledge of the main conformation of the peptide core opens the perspective to design possible inhibitors of peptide aggregation as a testing ground for future computational therapeutic strategies against amyloid diseases.

Acknowledgment. The author thanks P. Guenoun and A. Muenter for useful discussions.

Supporting Information Available: Coordinates for the peptide core in the folded state in solution in PDB format. This material is available free of charge via the Internet at http://pubs.acs.org.

References and Notes

(1) Soto, C. *CNS Drugs* **1999**, *12*, 347.
(2) Finder, V. H.; Glockshuber, R. *Neurodegener. Dis.* **2007**, *4*, 13.
(3) Matsuzaki, K.; Horikiri, C. *Biochemistry* **1999**, *38*, 4137.
(4) Schladitz, C.; Vieira, E. P.; Hermel, H.; Möhwald, H. *Biophys. J.* **1999**, *77*, 3305.
(5) Lepère, M.; Muenter, A. H.; Chevallard, C.; Guenoun, P.; Brezesinski, G. *Colloid Surf. A-Physicochem. Eng. Asp.* **2007**, *303*, 73.
(6) Kirkitadze, M. D.; Bitan, G.; Teplow, D. B. *J. Neurosci. Res.* **2002**, *69*, 567.
(7) Sacchettini, J. C.; Kelly, J. W. *Nat. Rev. Drug Discov.* **2002**, *1*, 267.
(8) Dumoulin, M.; Dobson, C. M. *Biochim.* **2004**, *86*, 589.
(9) van Gunsteren, W. F.; Bakowies, D.; Baron, R.; Chandrasekhar, I.; Christen, M.; Daura, X.; Gee, P.; Geerke, D. P.; Glättli, A.; Hünenberger, P. H. *Angew. Chem., Int. Ed.* **2006**, *45*, 4064.
(10) Simona, F.; Tiana, G.; Broglia, R. A.; Colombo, G. *J. Mol. Graph.* **2004**, *23*, 263.
(11) Daidone, I.; Simona, F.; Roccatano, D.; Broglia, R. A.; Tiana, G.; Colombo, G.; Di Nola, A. *Proteins* **2004**, *57*, 198.
(12) Han, W.; Wu, Y. D. *J. Am. Chem. Soc.* **2005**, *127*, 15408.
(13) Xu, Y. C.; Shen, J. J.; Luo, X. M.; Zhu, W. L.; Chen, K. X.; Ma, J. P.; Jiang, H. L. *Proc. Natl. Acad. Sci. U.S.A.* **2005**, *102*, 5403.
(14) Daidone, I.; Amadei, A.; Di Nola, A. *Proteins* **2005**, *59*, 510.
(15) Villa, A.; Mark, A. E.; Saracino, G. A. A.; Cosentino, U.; Pitea, D.; Moro, G.; Salmona, M. *J. Phys. Chem. B* **2006**, *110*, 1423.
(16) Wei, G. H.; Shea, J. E. *Biophys. J.* **2006**, *91*, 1638.
(17) Tomaselli, S.; Esposito, V.; Vangone, P.; van Nuland, N. A. J.; Bonvin, A. M. J. J.; Guerrini, R.; Tancredi, T.; Temussi, P. A.; Picone, D. *ChemBioChem* **2006**, *7*, 257.
(18) Khandogin, J.; Brooks, C. L. *Proc. Natl. Acad. Sci. U.S.A.* **2007**, *104*, 16880.
(19) Knecht, V.; Möhwald, H.; Lipowsky, R. *J. Phys. Chem. B* **2007**, *111*, 4161.
(20) Raffa, D. F.; Rauk, A. *J. Phys. Chem. B* **2007**, *111*, 3789.
(21) Urbanc, B.; Cruz, L.; Yun, S; Buldyrev, S. V.; Bitan, G.; Teplow, D. B.; Stanley, H. E. *Proc. Natl. Acad. Sci. U.S.A.* **2004**, *101*, 17345.
(22) Li, W. F.; Zhang, J.; Su, Y.; Wang, J.; Qin, M.; Wang, W. *J. Phys. Chem. B* **2007**, *111*, 13814.
(23) Valerio, M.; Colosimo, A.; Conti, F.; Giuliani, A.; Grottesi, A.; Manetti, C.; Zbilut, J. P. *Proteins* **2005**, *58*, 110.
(24) Flöck, D.; Colacino, S.; Colombo, G.; Di Nola, A. *Proteins* **2006**, *62*, 183.
(25) Luttmann, E.; Fels, G. *Chem. Phys.* **2006**, *323*, 138.
(26) Papanikolopoulou, K.; Schoehn, G.; Forge, V.; Forsyth, V. T.; Riekel, C.; Hernandez, J. F.; Ruigrok, R. W. H.; Mitraki, A. *J. Biol. Chem.* **2005**, *280*, 2481.
(27) van Raaij, M. J.; Mitraki, A.; Lavigne, G.; Cusack, S. *Nature* **1999**, *401*, 935.
(28) Zhang, F. *Angew. Chem., Int. Ed.* **2006**, *45*, 3611.
(29) Schuler, L. D.; Daura, X.; van Gunsteren, W. F. *J. Comput. Chem.* **2001**, *22*, 1205.
(30) Hermans, J.; Berendsen, H. J. C.; van Gunsteren, W. F.; Postma, J. P. M. *Biopolymers* **1984**, *23*, 1513.
(31) van der Spoel, D.; Lindahl, E.; Hess, B.; Groenhof, G.; Mark, A. E.; Berendsen, H. J. C. *J. Comput. Chem.* **2005**, *26*, 1701.
(32) Hess, B.; Bekker, H.; Berendsen, H. J. C.; Fraaije, J. G. E. M. *J. Comput. Chem.* **1997**, *18*, 1463.
(33) Feenstra, K. A.; Hess, B.; Berendsen, H. J. C. *J. Comput. Chem.* **1999**, *20*, 786.
(34) Feenstra, K. A.; Peter, C.; Scheek, R. M.; van Gunsteren, W. F.; Mark, A. E. *J. Biomol. NMR* **2002**, *23*, 181.
(35) Berendsen, H. J. C.; Postma, J. P. M.; van Gunsteren, W. F.; Di Nola, A.; Haak, J. R. *J. Chem. Phys.* **1984**, *81*, 3684.
(36) Darden, T.; York, D.; Pedersen, L. *J. Chem. Phys.* **1993**, *98*, 10089.
(37) Hünenberger, P. In *Simulation and theory of electrostatic interactions in solution: Computational chemistry, biophysics, and aqueous solutions*; Pratt, L., Hummer, G., Eds.; American Institute of Physics, 1999; pp 17−83.
(38) Kabsch, W.; Sander, C. *Biopolymers* **1983**, *22*, 2577.
(39) Daura, X.; Gademann, K.; Jaun, B.; Seebach, D.; van; Gunsteren, W. F.; Mark, A. E. *Angew. Chem., Int. Ed.* **1999**, *38*, 236.
(40) Connolly, M. L. *Science* **1983**, *221*, 709.
(41) Humphrey, W.; Dalke, A.; Schulten, K. *J. Mol. Graph.* **1996**, *14*, 33.
(42) Koradi, R.; Billeter, M.; Wüthrich, K. *J. Mol. Graph.* **1996**, *14*, 51.
(43) Zhou, R. H.; Berne, B. J.; Germain, R. *Proc. Natl. Acad. Sci. U.S.A.* **2001**, *98*, 14931.
(44) Pike, C. J.; Walencewiczwasserman, A. J.; Kosmoski, J.; Cribbs, D. H.; Glabe, C. G.; Cotman, C. W. *J. Neurochem.* **1995**, *64*, 253.
(45) Findeis, M. A. *Pharmacol. Ther.* **2007**, *116*, 266.
(46) Lepère, M.; Chevallard, C.; Hernandez, J. F.; Mitraki, A.; Guenoun, P. *Langmuir* **2007**, *23*, 8150.
(47) Koshland, D. E. *Angew. Chem., Int. Ed. Engl.* **1995**, *33*, 2375.
(48) van Gunsteren, W. F.; Burgi, P.; Peter, C.; Daura, X. *Angew. Chem., Int. Ed.* **2001**, *40*, 351.

JP8026513